CHAPTER III
RESEARCH METHODOLOGY

Research methodology presents the Quantum Diamond Spectrometer setup consisting of an optical system and an electronic system. Subsequently, we illustrate signal detection via optically detected magnetic resonance (ODMR) pulse sequences. The pulse sequences involve a microwave generator to sweeping and determine the magnitude and orientation of the magnetic field. Ultimately, we will briefly examine the utilization of magnetic field computations in vector magnetometry and magnetic field mapping.

3.1 Quantum Diamond Spectrometer or QDS

Confocal microscopes are commonly employed in investigations with NV due to their ability to provide high-resolution imaging and to facilitate convenient selection of focusing settings. For instance, confocal microscopes can conduct NV center scanning probes, providing a magnetic field image of 30 nm iron oxide nanoparticles with a spatial resolution of 100 nm (Mosavian et al., 2024). The confocal microscope is also used to study charge conversion of the NV center (Wood et al., 2024). A confocal microscope with an NV center can also be used to study atomic thermometers for biochemical purposes, with a sensitivity of up to 80 mK/Hz. This technique allows researchers to conduct biochemical studies at the femtoliter scale (Li et al., 2024).

However, confocal microscopes take a long time to scan and can hardly track high-speed changes in magnetic fields. Due to rapid changes in capabilities and straightforward optical alignment, we employ the Quantum Diamond Spectrometer (QDS) (Bucher et al., 2019) to achieve high spatial resolution for material characterization. For instance, the QDS offers enhanced fluorescence signals, thereby decreasing data acquisition time and improving spatial resolution for sensor applications. In addition, QDS functions similarly to

nuclear magnetic resonance (NMR) spectroscopy. We use NMR spectroscopy to characterize elements within a substance. In the case of QDS, it is utilized to sense magnetic fields in solid or liquid matter with femtomole sensitivity (Li et al., 2022). The QDS consists of an optical system and an electronic system. The optical system excites electrons in the NV center. The electronic system controls electrons at an energy level transitions.

3.1.1 Optical system

The optical system is used to excite the NV center in Figure 3.1. The system uses a 532 nm green laser as a light source (Coherent OBIS 532 nm). The laser is focused by a convex lens with a focal length of 100 mm (Thorlabs AC254-100-A) to pass through an Acousto-Optic Modulator (AOM) (Gooch & Housego AOMO 3080-120). The AOM creates a diffraction pattern through piezoelectric vibration. The diffracted laser passes to a diaphragm (Thorlabs ID37Z) to create a switch from the diffraction pattern. The first order and zeroth diffraction patterns are defined to be “on” and “off” states. The zeroth-order diffraction pattern is blocked by the diaphragm and the first diffraction pattern passes the diaphragm. The first-order diffraction beam passes through a polarizer and a half-wave plate (HWP). The polarizer and HWP control polarization of the laser before the diamond. The polarized beam is demagnified beam size by beam reducer: a convex lens with a focal length of 200 mm (Thorlabs AC254-200-A) and a convex lens with a focal length of 30 mm (Thorlabs AC254-030-A). The laser is flipped upward to the diamond on the light guide (Edmund optics stock number 49-402) and is focused by a convex lens with a focal length of 50 mm (Thorlabs AC254-050-A). The focused laser passes through the light guide to the diamond and goes out from the other side due to total internal reflection. The red fluorescence from the diamond goes through the light guide to the avalanche photodetector (APD) (Laser components A-CUBE-S3000-03). The APD places two filters before the detector, one to block the green laser (Thorlabs NF533-17) and the other to select the desired wavelength (Thorlabs FELH0600). Then, the APD signal is sampled by

NI-DAQ (National Instruments PCIe-6363) and sent to the computer for processing and calculating data.

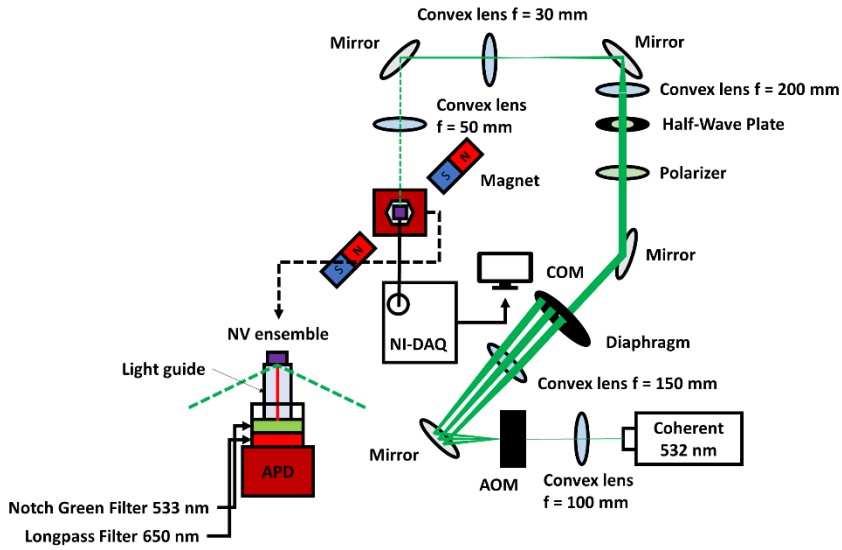

Figure 3.1 Quantum Diamond Spectrometer (QDS) schematic.

3.1.2 Electronics system

The electronics system controls RF output from the signal generator to the microwave loop to manipulate the electron spin states of the NV center, as shown in Figure 3.2. The signal is generated by a microwave source (RIGOL DSG836) and sent to a microwave switch (Mini-circuits ZASWA-2-50DRA+). The switch controls the RF signal to the microwave loop by a transistor-transistor logic (TTL) signal from PulseBlaster (PulseBlaster ESR-Pro-500). The switch has 2 output ports consisting of OUT1, the first port, and OUT2, the second port. When the TTL signal is in a high state, radio frequency (RF) impulses are received through the RF-IN port and subsequently transmitted over the OUT2 channel. Another output port, denoted as OUT1, is terminated with a 50-ohm impedance (Mini-circuits ANNE-50+) to prevent the generation of reflected signals. The signals in the OUT2 channel undergo a high-pass filter (Mini-Circuits VHF-1600+) for noise filtering and are amplified by an amplifier (Mini-Circuits ZHL-16W-43-S+). An attenuator (Mini-Circuits VAT-10A+) is added before the amplifier to protect the amplifier from damage. The amplified

signal is driven to a circulator (Ditom D3C2040) before reaching the microwave loop to protect the amplifier from potential harm, while the reflected signal on the circulator is ended by a terminator. Finally, the microwave loop sends signals to the diamond.

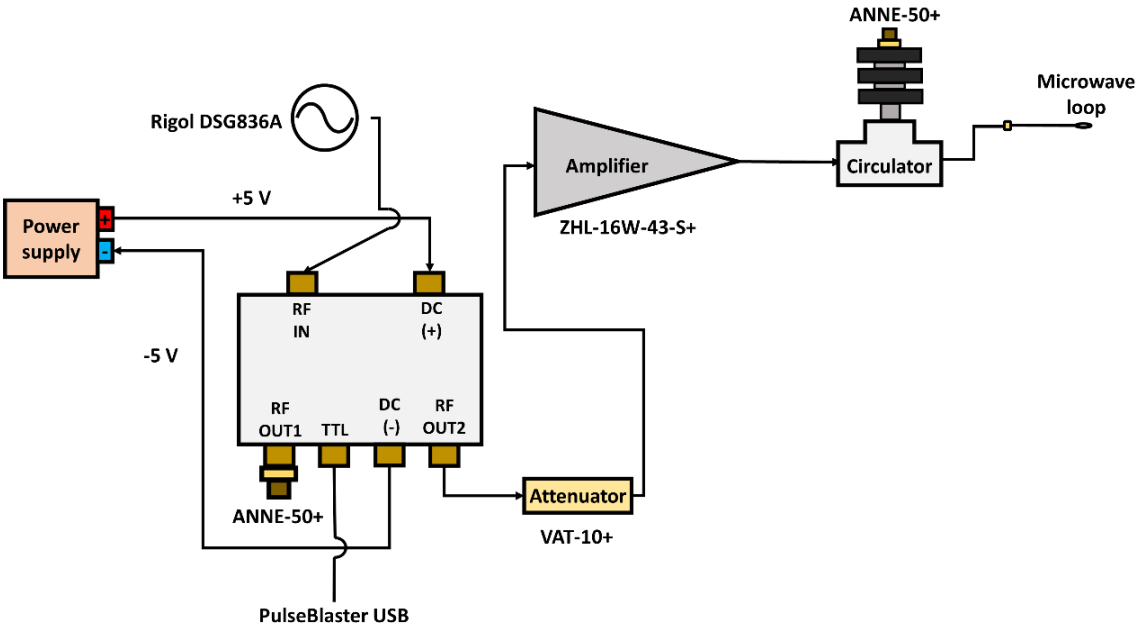

Figure 3.2 Electronic diagram for controlling microwave.

3.2 Pulse sequence

Electrons are controlled to occupy the desired energy level with pulse sequences. The pulse sequence creates each pulse with each duration for specific instruments. As a result, pulse duration relates to manipulating electrons in experiments.

3.2.1 Optically Detected Magnetic Resonance (ODMR)

Optically Detected Magnetic Resonance (ODMR) is an integration of electron spin resonance (ESR) and optical measurements. ODMR can represent the relation between optical measurement and microwave frequency. The ODMR pulse sequence uses 3 components: a 532-nm laser (“Green”), microwave (“MW”), and avalanche photodetector (“APD”) in figure 2.5. The ODMR pulse sequence consists of 2 sequences, continuous wave

(CW) ODMR and pulsed ODMR. CW ODMR is a measurement technique releasing continuous microwave and laser. In the figure 2.5A, we start with “Green” turning the laser on and “MW” turning the microwave on. Following that, there is waiting time to turn on “APD” for detection. In the end, it will go back to the initial point and continue the loop with “n” rounds. For the second loop, it is reference detection due to no “MW”. Pulsed ODMR is a rhythmic signal transmission in figure 2.5B. The pulse sequence begins with "Green" turning on the laser for the "Initialization time" for NV polarization. In this process, electrons at a mixed state are polarized to $m_s = 0$ for state preparation. After that, the laser is turned off to repolarize the condition during "relaxation time". After that, the microwave is turned on to excite electrons from $m_s = 0$ to $m_s = 1$ throughout the "Microwave time" duration. After that, "APD" detects signals within the detection range of "Pulsewidth". At the end of green, it will return to the beginning and repeat the loop with "n" rounds. The first loop detects signals. Because there is no microwave, the second loop detects reference signals. We combine data from signal and reference detection to split it for photoluminescence.

The difference between CW ODMR and pulsed ODMR is pulse. CW ODMR releases microwave and laser continuously. The continuous release makes a wider linewidth due to laser repumping and microwave broadening over the whole experiment, which leads to low sensitivity (Levine et al., 2019). The effect is reduced by employing lock-in detection with strong laser and microwave intensity instead (Barry et al., 2020). Pulsed ODMR, on the other hand, uses appropriate duration for laser initialization, microwave manipulation, and readout to reduce repumping and power broadening effects. Separation makes electrons repolarize the state efficiently for the next initialization causing a linewidth reduction (Levine et al., 2019). The narrow linewidth indicates higher sensitivity because it distinguishes splitting correctly. In addition, the pulse duration for operating the pulsed ODMR experiment relating to pulsed ODMR in Figure 3.3 is in table 2.1.

After adjusting pulse duration and establishing setup, we find the resolution of setup through ODMR sequence. The resolution is the full-width half maximum (FWHM) of

a dip in Zeeman splitting. In this case, the first dip is used to find the FWHM. So, the resolution is 26 MHz in figure 3.4.

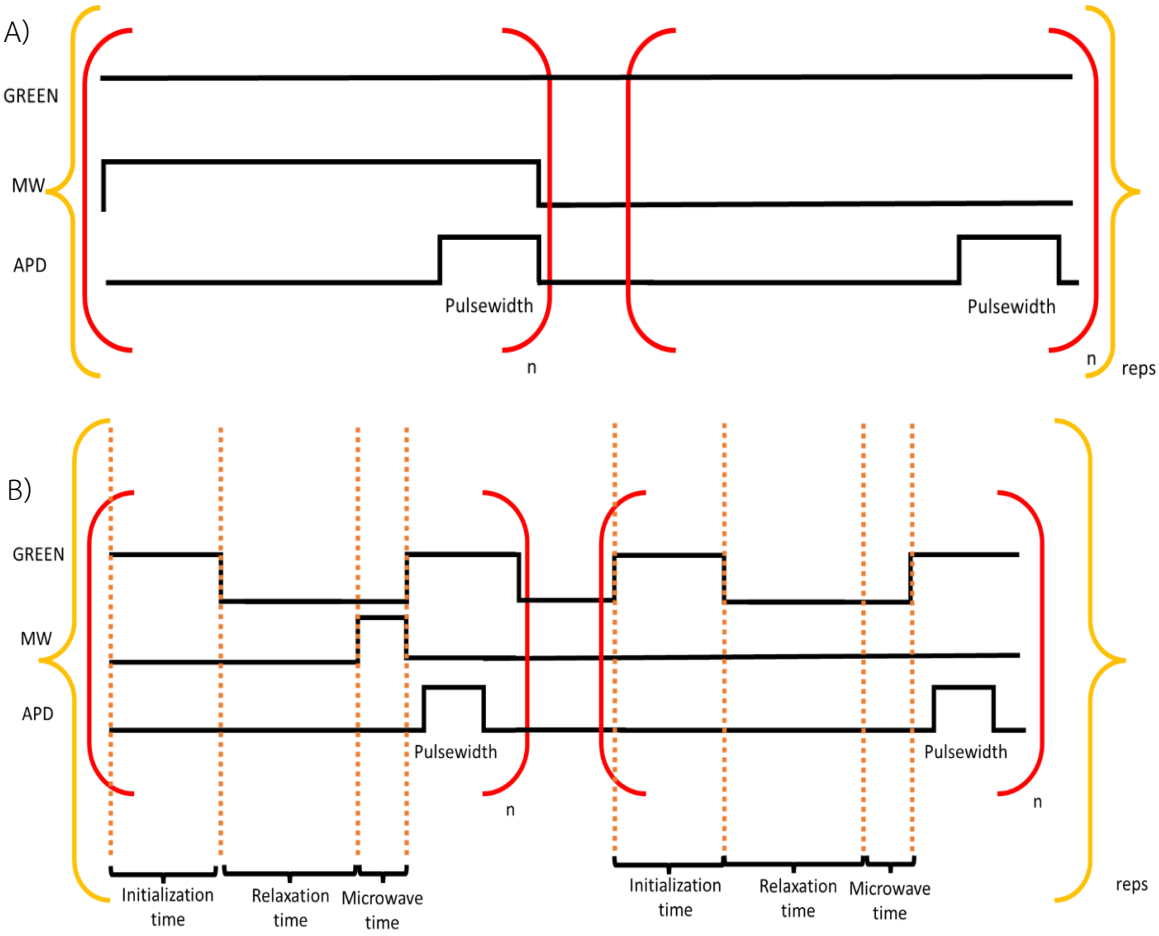

Figure 3.3 ODMR sequence is designed to find the position of an energy level of a NV for control sequence. Figure A) is Continuous Wave (CW) ODMR. Figure B) is pulsed ODMR.

Table 2.1 Pulse duration for Pulsed ODMR.

Name	Duration
Initialization time	3 – 5 microseconds
Relaxation	1 – 5 microseconds
MW time	0.05 – 1 microseconds
Pulsewidth	-

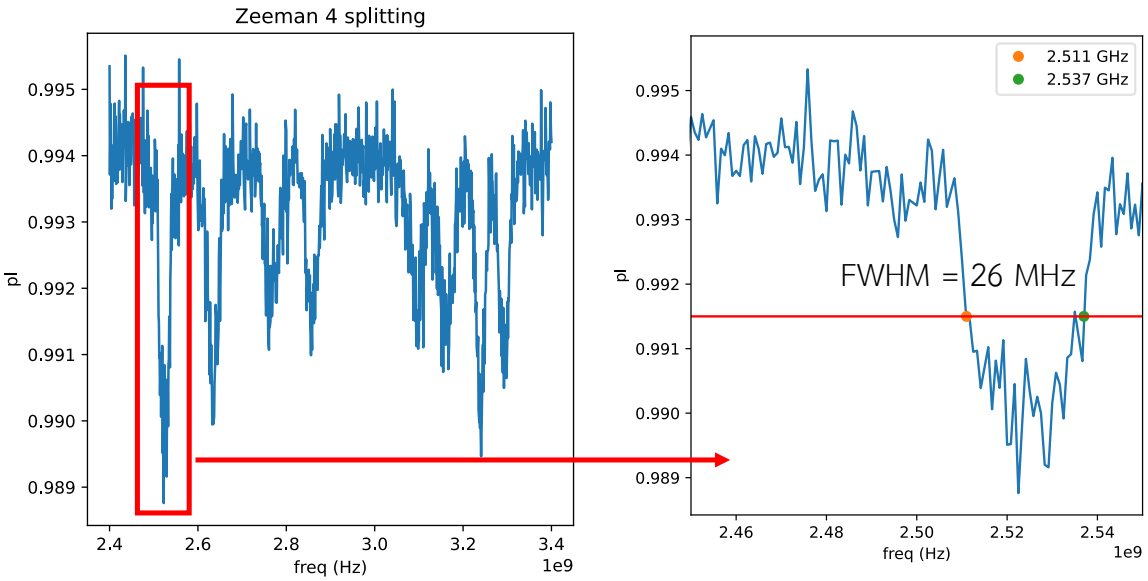

Figure 3.4 The full width half maximum (FWHM) of system is 26 MHz with using the first dip of Zeeman 4 splitting.

3.3 Microwave generator

To manipulate electrons in the NV center, radio-frequency (RF) signals are required to excite electrons from the ground state. These RF signals are generated by a microwave generator (Rigol DSG836), which offers a tunable power range from -100 dBm to +20 dBm, a maximum frequency of 3.6 GHz, and a frequency resolution of 0.01 Hz.

This thesis aims to demonstrate high-speed vector magnetometry. The microwave source supports real-time or near real-time signal generation via its frequency-sweeping function, capable of transmitting RF signals at intervals of 50 ms per frequency step.

3.4 Determining magnetic field magnitudes and orientations

The determination focuses on the detecting signal process and automation program development. Following that, the magnetic field magnitude and orientation calculation are presented.

3.4.1 Signal detection process

The fluorescence signal from the diamond is continuously emitted and directed to the detector. Accurate detection of this signal is achieved using an ODMR pulse sequence, which requires precise timing of control pulses.

A Pulse Blaster is employed to generate these control pulses and to synchronize the operation of four key instruments: the Acousto-Optic Modulator (AOM), an RF switch, a Data Acquisition (DAQ) system, and a microwave (MW) source. The Pulse Blaster sends signals through four output ports:

- The first port (PB0) triggers the AOM to produce a diffraction pattern that modulates the optical path.
- The second port (PB1) activates the RF switch, allowing RF signals from the MW source to pass through.
- The third port triggers (PB2) the DAQ system to record fluorescence data during the pulse sequence. In this experiment, data is collected with a single trigger per sequence, rather than over a periodic interval.
- Finally, the fourth port (PB3) initiates the frequency sweep of the MW source, enabling controlled release of microwave signals.

3.4.2 Program

The program in Figure 3.3 is designed by Qtdesigner software. The software uses to designing and building graphical user interfaces and is outlined by the microwave generator interface of sweeping program. The program consists of 3 functions: Sweep function, Sweep parameter, and ODMR parameters for setting before starting the experiment.

3.4.2.1 Sweeping function

The sweeping functions in this box are commands that set the microwave source, preparing the system before releasing the signal and waiting for the trigger signal from the external pulse.

3.4.2.2 Sweeping parameters

In this box, the sweeping parameters contain free parameters to adjust sweeping range, such as setting initial and stop frequency for sweeping frequency, microwave power range with setting initial and stop microwave power for sweeping levels, the number of microwave frequencies per sweeping, and the shape of the sweeping signal.

3.4.2.3 ODMR parameters

The ODMR parameters in this box set the pulse duration, including initialization time, relaxation time, microwave time, number of samples, and repetition.

Figure 3.5 The Sweeping program is designed by Qtdesigner. The program has three main parts “Sweep function”, “Sweep parameter” and “ODMR parameter”.

3.4.3 Magnetic field calculation

The magnitude and direction of a magnetic field can be extracted from the ODMR signal by analyzing its frequency splitting behavior. In this system, the external magnetic field interacts with the NV centers in diamond, specifically affecting the spin states of electrons. This interaction leads to a characteristic splitting in the ODMR spectrum, which can be used to determine both the field magnitude and its spatial orientation.

For simplicity, the interaction is first illustrated with respect to a single NV axis, as shown in Figure 3.4 The external magnetic field B forms an angle α with this NV axis. The magnetic field causes a Zeeman splitting of the energy levels, resulting in two resonant frequencies in the ODMR signal. Using this splitting, the magnetic field's magnitude and orientation can be derived from Eq. 3 and Eq. 4 originated from eigenvalues of NV Hamiltonian.

Eq. 3 calculates the magnetic field magnitude, while Eq. 4 determines the field orientation. These expressions are derived from the eigenvalue solutions of the NV center's spin Hamiltonian. The magnitude B is calculated based on the frequency difference between the two ODMR peaks (w_1 and w_2), the zero-field splitting constant D, and the NV center's gyromagnetic ratio γ_{NV}. The angle α represents the angle between the NV axis and the magnetic field direction.

The calculated magnetic field magnitude represents the component of the field acting along a single NV axis. Since the NV center has four crystallographic orientations, the full magnetic field vector can be reconstructed by averaging the results from all four axes. This provides a more comprehensive representation of the magnetic field acting on the NV center

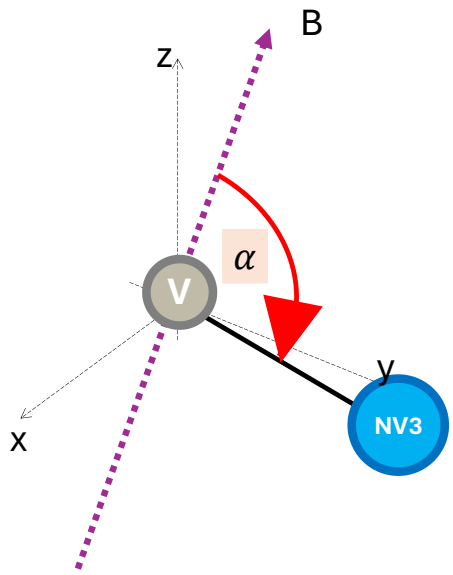

Figure 3.6 An NV axis and magnetic field in the system. The angle between the magnetic field and an NV axis is called alpha and is calculated by Eq. 4.

$$B = \frac{\sqrt{(w_1^2 + w_2^2 - w_1 w_2 - D^2)/3}}{\gamma_{NV}}, \quad \text{Eq. 3}$$

$$\alpha = \arccos\left(\pm \sqrt{\frac{(2w_1 - w_2 - D)(w_1 - 2w_2 + D)(w_1 + w_2 + D)}{[9D({w_1}^2 - w_1 w_2 + {w_2}^2 - D^2)]}} \right). \quad \text{Eq. 4}$$

While the direction of the magnetic field is inferred through the angular relationship α with respect to the NV axis, it does not uniquely determine systematic magnetic field direction. So, the set of all vectors forming the same angle α with an NV axis defines a cone surface, and thus the possible magnetic field directions lie on this conical surface. Due to vector symmetry, both positive and negative field directions result in two cones per NV axis.

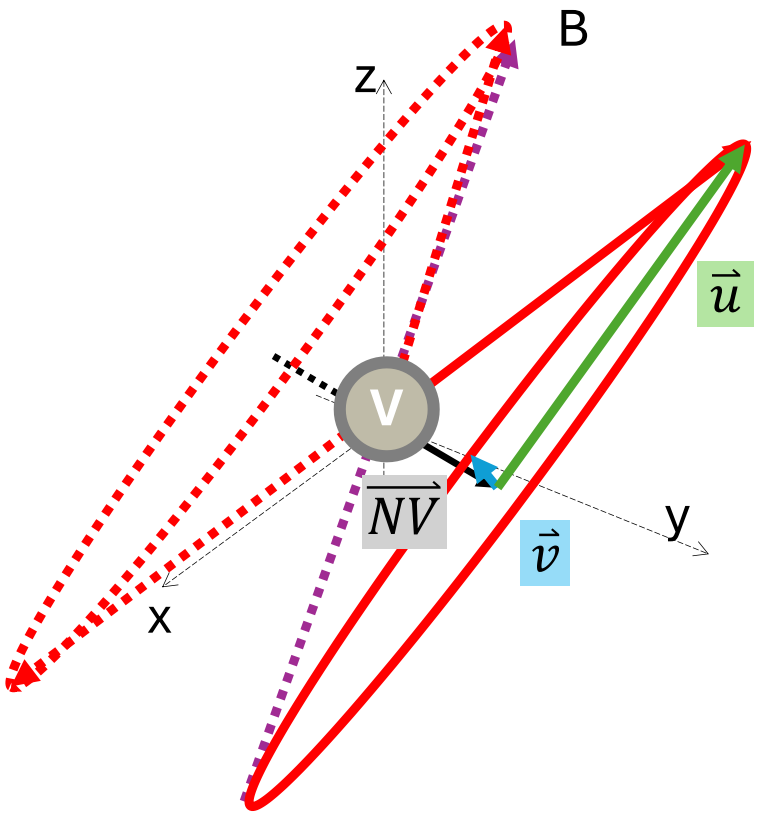

Figure 3.7 The two cones represent possible magnetic field directions to act on an NV axis. The cone surface is described mathematically by orthogonal vector between $\vec{u}$ (blue vector) and $\vec{v}$ (green vector) constraining both vectors are perpendicular with the NV axis or $\overrightarrow{NV}$ (black vector) and each other.

To mathematically describe this surface like Figure 3.5, two orthogonal $\vec{u}$ and $\vec{v}$ are introduced. These vectors are perpendicular to the NV axis and to each other, forming a local coordinate system for the cone. $\vec{u}$ is obtained by solving the dot product in Eq. 5.

$$\overrightarrow{NV} \cdot \vec{u} = 0 \quad \text{Eq. 5}$$

$$\overrightarrow{NV} = [NV_x, NV_y, NV_z], \quad \vec{u} = [u_x, u_y, u_z] \quad \text{Eq. 6}$$

$$So, \quad 0 = [NV_x, NV_y, NV_z] \cdot [u_x, u_y, u_z] \quad \text{Eq. 7}$$

$$From\ Eq.\ 5, \quad 0 = NV_x u_x + NV_y u_y + NV_z u_z \quad \text{Eq. 8}$$

$$From\ Eq.6,\ \ if\ u_z = 0,\ \ u_x = -NV_y\ and\ u_y = NV_x$$
$$\therefore \quad \vec{u} = [u_x, u_y, u_z] = [-NV_y, NV_x, 0] \quad \text{Eq. 9}$$

This condition ensures orthogonality. Multiple solutions can satisfy this condition, but for simplicity, the component u_z is set to zero. This leads to the explicit form of $\vec{u}$ in Eq. 9. The second orthogonal $\vec{v}$ is obtained via the cross product of $\overrightarrow{NV}$ and $\vec{u}$, as given in Eq. 10. The resulting $\vec{v}$ is normalized in Eq. 11, ensuring unit length for consistent directional analysis. Finally, both $\vec{u}$ and $\vec{v}$ are normalized to form a basis for constructing direction vectors on the cone's surface, as shown in Eq. 12.

$$\vec{v} = \vec{u} \times \overrightarrow{NV} \quad \text{Eq. 10}$$

$$\vec{v} = [-NV_y, NV_x, 0] \times [NV_x, NV_y, NV_z]$$
$$\therefore \quad \vec{v} = [NV_x NV_z, NV_y NV_z, -{NV_x}^2 - {NV_y}^2] \quad \text{Eq. 11}$$

$$\therefore \quad \hat{u} = \frac{[-NV_y, NV_x, 0]}{\sqrt{(-NV_y)^2 + {NV_x}^2 + 0^2}},$$
$$\hat{v} = \frac{[NV_x NV_z, NV_y NV_z, -{NV_x}^2 - {NV_y}^2]}{\sqrt{(NV_x NV_z)^2 + (NV_y NV_z)^2 + (-{NV_x}^2 - {NV_y}^2)^2}} \quad \text{Eq. 12}$$

A special set of vectors on the cone surface, whose component on the NV axis is constrainted to 1, representing a possible magnetic field direction, is then expressed as:

$$\therefore \widehat{NV} + (\hat{u} \sin t + \hat{v} \cos t) \tan \alpha = [x, y, z] \quad \text{Eq. 13}$$

where t is a free parameter sweeping from $-\pi$ to π on the cone plane. The result is a set of magnetic field direction vectors in Cartesian coordinates relative to the NV frame. These coordinates are then transformed into the laboratory frame and can be converted into spherical coordinates using trigonometric relationships. The resulting angles— θ (inclination) and ϕ (azimuth)—are given in Eq. 14 and 15.

$$\theta = \cos^{-1}\frac{z}{\sqrt{x^2+y^2+z^2}} \quad \text{Eq. 14}$$

$$\phi = \tan^{-1}\frac{y}{x} \quad \text{Eq. 15}$$

Each NV axis produces two possible directional curves (positive and negative cones) in spherical coordinates. These solution sets can be visualized as lines on a spherical surface, as shown in Figure 3.6. Consequently, a single NV axis provides two possible cones of magnetic field solutions.

In a typical NV center, there are four different crystallographic orientations. Each orientation yields its own pair of solution cones in Figure 3.7. When all four solution sets are combined, their intersections correspond to the actual direction of the magnetic field. This intersection analysis is illustrated in Figure 3.8. By identifying the common intersection among the four solution sets, both the orientation and magnitude of the external magnetic field acting on the NV center can be accurately determined.

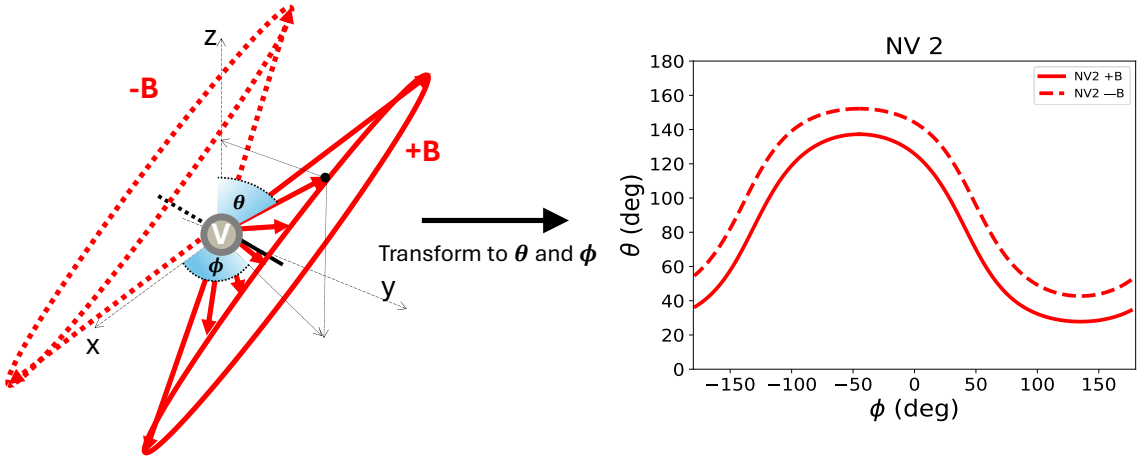

Figure 3.8 Transformation from Cartesian coordinate to spherical coordinate using trigonometry. The answer set in the graph represents positive and negative magnetic field orientation possibilities that act on the NV axis.

3.4.4 Experimental workflow

The section presents experiments that validate the setup's ability to detect signals accurately and the precision of the magnetic field calculations in determining orientation and magnitude. First, the QDS detects signals from ODMR. The ODMR signal is then analyzed through simulation to examine NV excitation. Next, the magnetic field calculation is tested using simulations, raw ODMR data, and specific test cases. Finally, the magnetic field calculation is integrated with QDS to perform vector magnetometry, demonstrating both the orientation and magnitude of the magnetic field.

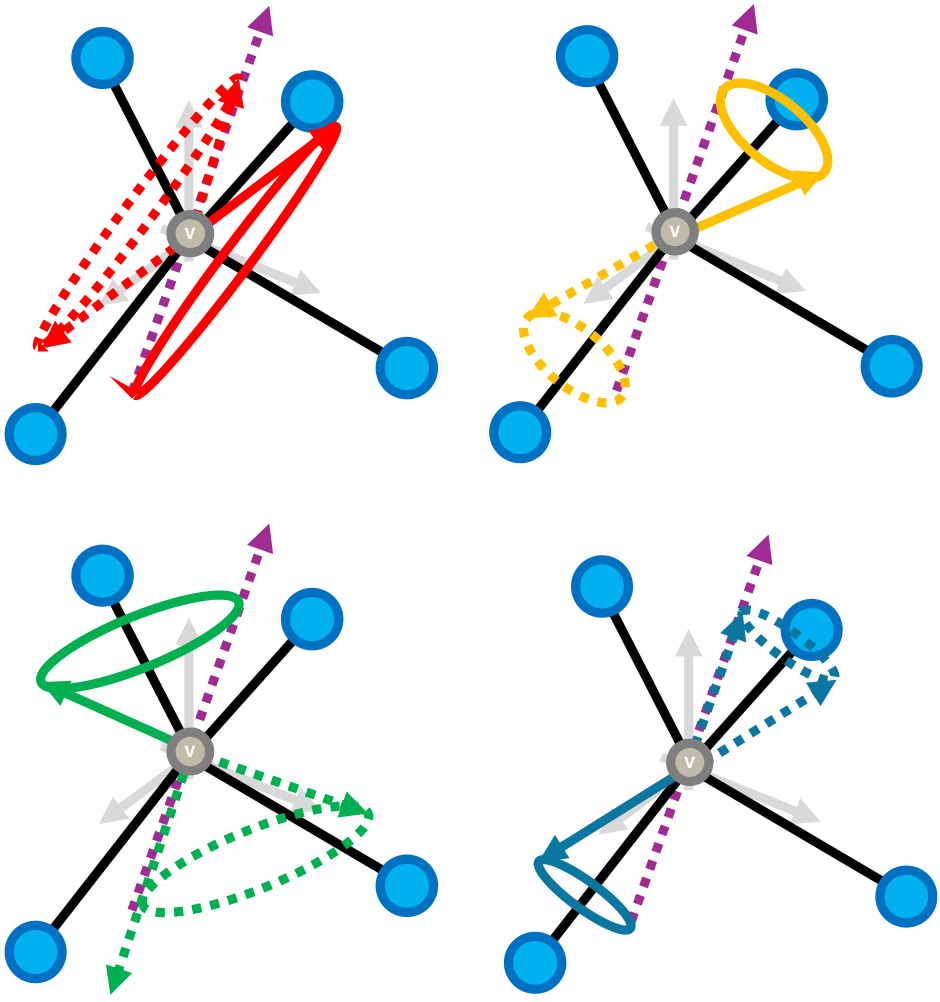

Figure 3.9 The 4 orientations of the NV center senses magnetic field in the specific direction and create cones along NV axes.

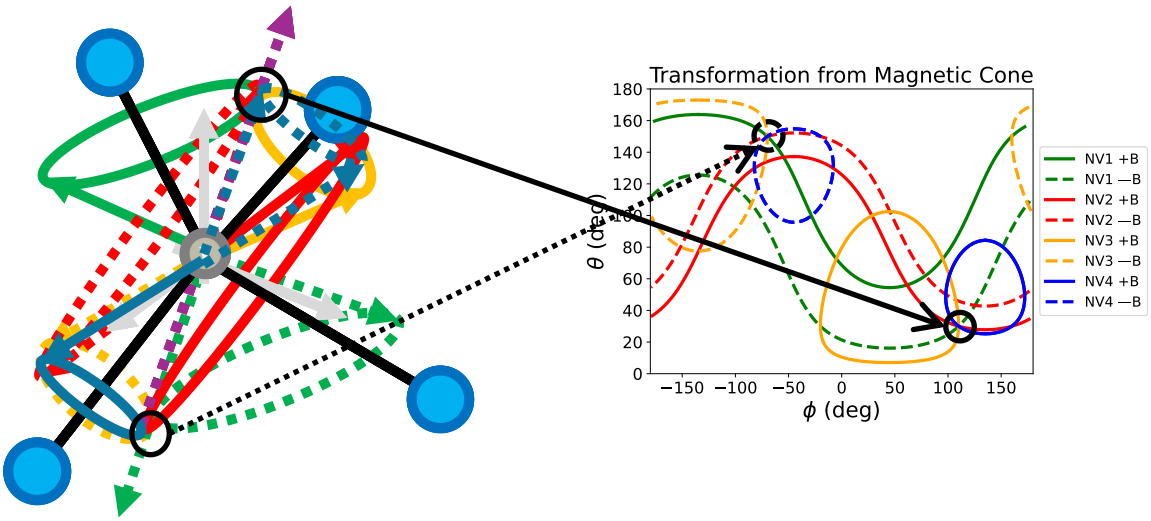

Figure 3.10 3D and 2D graphs represent that answer sets of 4 NV axes are not unique and have interceptions. The interceptions show real magnetic field direction acting on the NV center in positive and negative field.